Journal of Mathematical Imaging and Vision manuscript No.
(will be inserted by the editor)

Cortical-inspired Wilson-Cowan-type equations for orientation-dependent contrast perception modelling

Marcelo Bertalmío · Luca Calatroni · Valentina Franceschi · Benedetta Franceschiello · Dario Prandi

Received: date / Accepted: date

Abstract We consider the evolution model proposed in [9,6] to describe illusory contrast perception phenomena induced by surrounding orientations. Firstly, we highlight its analogies and differences with widely used Wilson-Cowan equations [48], mainly in terms of efficient representation properties. Then, in order to explicitly encode local directional information, we exploit the model of the primary visual cortex V1 proposed in [20] and largely used over the last years for several image processing problems [24,38,28]. The resulting model is capable to describe assimilation and contrast visual bias at the same time, the main novelty being its explicit dependence on local image orientation. We report several numerical tests showing the ability of the model to explain, in particular, orientation-dependent phenomena such as grating induction and a modified version of the Poggendorff illusion. For this latter example, we empirically show the existence of a set of threshold parameters differentiating from inpainting to perception-type reconstructions, describing long-range connectivity between different hypercolumns in the primary visual cortex.

Keywords Wilson-Cowan equations · Primary Visual Cortex · Orientation-dependent modelling · Contrast Perception · Variational modelling · Geometrical optical illusions

LC, VF and DP acknowledge the support of a public grant overseen by the French National Research Agency (ANR) as part of the *Investissement d'avenir program*, through the iCODE project funded by the IDEX Paris-Saclay, ANR-11-IDEX-0003-02 and of the research project *LiftME* funded by INS2I, CNRS. VF and DP also acknowledge the support of ANR-15-CE40-0018 project *SRGI - Sub-Riemannian Geometry and Interactions*. BF acknowledges the support of the Fondation Asile des Aveugles.

Marcelo Bertalmío
DTIC, Universitat Pompeu Fabra, Barcelona, Spain
marcelo.bertalmio@upf.edu

Luca Calatroni
Université Côte dAzur, CNRS, Inria, I3S, France
calatroni@i3s.unice.fr

Valentina Franceschi
LJLL, Sorbonne Université, Paris, France
franceschiv@ljll.math.upmc.fr

Benedetta Franceschiello
Fondation Asile des Aveugles and LINE, Dep. of Radiology, CHUV, Lausanne, Switzerland
benedetta.franceschiello@fa2.ch

Dario Prandi
CNRS, L2S, CentraleSupelec, Gif-sur-Yvette, France
dario.prandi@centralesupelec.fr

1 Introduction

Recent studies on vision research have shown that many, if not most, popular vision models can be described by a cascade of linear and non-linear (L+NL) operations [33]. This is the case for several reference models describing visual perception - e.g. the Oriented Difference Of Gaussians (ODOG) [12] or the Brightness Induction Wavelet Model (BIWaM) [36] - and, analogously, for models describing neural activities [18]. These L+NL models are suitable in many cases for describing retinal and thalamic activity, but they have been shown to have low predictive power for modelling the neural activity in the primary visual cortex (V1), explaining less than 40% of the variance of the data [18].

Furthermore, there exist several models in vision research which are not in the aforeementioned form of (L+NL) operations. Prominent examples are, for instance, models describing neural dynamics via Wilson-Cowan equations [48,16]. These equations describe the activation state $a(\xi, t)$ of a population of neurons at

time $t > 0$ with V1 coordinates $\xi = (x, \theta)$, where $x \in \mathbb{R}^2$ is the spatial preference and $\theta \in \mathbb{P}^1 \simeq [0, \pi)$ is the orientation preference, via the following ODE:

$$\frac{\partial}{\partial t} a(\xi, t) = -\alpha a(\xi, t) + \nu \int_{\mathbb{R}^2 \times \mathbb{P}^1} \omega(\xi \| \xi') \sigma(a(\xi', t))\, d\xi' + h(\xi, t). \quad (1)$$

Here, $\alpha, \nu > 0$ are fixed parameters, $\omega(\xi \| \xi')$ is a kernel modelling the interaction at two different locations ξ and ξ', $\sigma : \mathbb{R} \to \mathbb{R}$ is a non-linear sigmoid saturation function and h represents the external stimulus. Wilson-Cowan models in the form (1) have been extensively studied within the neurosciences community to describe cortical low-level dynamics, see, e.g. [21]. However, their use in the context of psychophisics as a tool to describe, for instance, visual illusions has been considered only recently by the authors in [7], where a discussion on the lack of a variational counterpart for model (1) is given.

In [9,10,6] the authors show how a slight, yet effective, modification of the Wilson-Cowan equation that does not consider orientation admits a variational formulation through an associated energy functional which can be linked to histogram equalisation, visual adaptation and the efficient representation principle, an important school of thought in vision science [35]. This principle, introduced by Attneave [2] and Barlow [4], is based on viewing neural systems through the lens of information theory and states that neural responses aim to overcome neurobiological constraints and to optimise the limited biological resources by self-adapting to the statistics of the images that the individual typically encounters, so that the visual information can be encoded in the most efficient way. Natural images (and, more generally, images in urban environments) are in fact not random arrays of values, since they present a significant statistical structure. With respect to such statistics, nearby points tend to have similar values; as a result, there is significant correlation among pixels, with a redundancy of 90% or more [1], and it would be highly inefficient and detrimental for the visual system to simply encode each pixel independently. Another very important reason to remove redundant statistical information from the representation is that the statistical rules impose constraints on the image values that are produced, preventing the encoded signal from utilizing the full capacity of the visual channel, which is another inefficient or even wasteful use of biological resources. By removing what is redundant or predictable from the statistics of the visual stimulus, the visual system can concentrate on what's actually informative [39]. Remarkably, the efficient representation principle has correctly predicted a number of neural processing aspects and phenomena, and is the only framework able to predict the functional properties of neurons from a very simple principle. In [1], Atick makes the point that one of the two different types of redundancy or inefficiency in the visual system is the one that happens if some neural response levels are used more frequently than others: for this type of redundancy, the optimal code is the one that performs histogram equalisation, which can be obtained by means of the aforementioned modification of the WC model (1).

Contribution The first contribution of this paper is to formally prove that in a continuous setting Wilson-Cowan equations are non-variational, and for this reason their solutions do not provide a representation as efficient as the modification corresponding to local histogram equalisation.

Next, we introduce an explicit orientation dependence into this modification via a lifting procedure inspired by neuro-physiological models of V1 [20,24,38] and their applications to image processing [14,50]. The lifting procedure, illustrated in Figure 1, consists in associating to each point of the retinal plane $x \in \mathbb{R}^2$ the tangent direction θ of the contour at point x, thus 'lifting' the retinal plane $\mathbb{R}^2$ within the feature space $\mathbb{R}^2 \times \mathbb{P}^1$ of positions and orientations. This mathematical construction mimics the neural representations of the image features that the cortex performs, according to well-known studies in vision science such as the one by Hubel and Wiesel [30].

Following the preliminary version of this work [8], we then report some numerical evidence showing how the proposed model is able to better reproduce some visual perception bias than both its orientation independent version, and state-of-the-art (L+NL) models describing visual perception. In particular, after reporting some numerical results for classical non-orientation-dependent illusions, we test our model on orientation-dependent Grating Induction (GI) phenomena (generalising the ones presented in [12, Figure 3], see also [34]) and show a direct dependence of the output image on the orientation, which cannot be reproduced via orientation-independent models.

We then test the proposed model on a modified version of the Poggendorff illusion, a geometrical optical effect where a misalignment of two collinear segments is induced by the presence of a surface [45,46], see Figure 12. For this modified version, our model is able to nicely integrate the feature of contrast with respect to the state-of-the-art models for the classical phenomenon, such as those based on filtering techniques, [12,36], those based on the statistics of natural

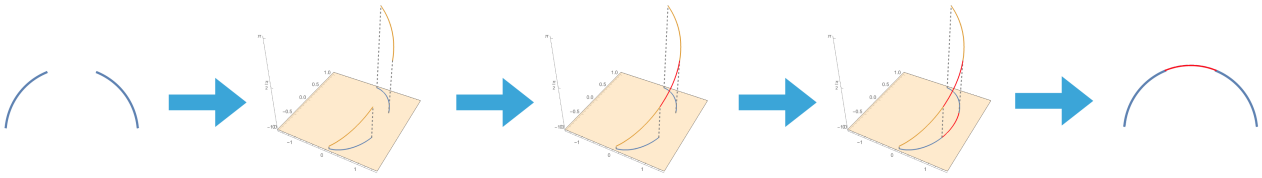


Fig. 1: Pipeline for cortical-inspired image processing: Each $x \in \mathbb{R}^2$ is lifted in the space $\mathbb{R}^2 \times \mathbb{P}^1$ according to the correspondent tangent direction of the curve at point x. In the lifted space, many operations can be performed, such as completion of missing paths of the initial curve. Then, the information retrieved within the lifted space can be reprojected onto the $\mathbb{R}^2$ plane.

images [29], and different cortical-based ones [26,27]. Moreover, we also show that such feature is not correctly integrated by the classical Wilson-Cowan equations (1), even if orientation-dependent.

Finally, for the Poggendorff illusion, we extend the numerical discussion in [8] by further reporting an empirical study concerning the sensitivity of the model to some parameters, which evidences the existence of threshold values able to change the nature of the completion properties of the model, e.g. to make it switch from inpainting type (geometrical completion) to perception type (perceptual completion).

2 Variational and evolution methods in vision research

The use of variational methods for solving ill-posed imaging problems is nowadays very classical within the imaging community. For a given degraded image f and a (possibly non-linear) degradation operator $\mathcal{T}$ describing noising, blurring and-or under-sampling phenomena, the solution of the problem

$$\text{find } u \quad \text{s.t.} \quad f = \mathcal{T}(u) \tag{2}$$

often lacks fundamental properties such as existence, uniqueness and stability, requiring alternative strategies to be used in order to reformulate the problem in a well-posed way.

In variational regularisation approaches, for instance, one looks for an approximation $u_\star$ of the real solution u by solving a suitable optimisation problem, so that

$$u_\star \in \arg\min \mathcal{E}(u), \tag{3}$$

where $\mathcal{E}$ is a (possibly non-convex) energy functional which typically combines prior information available both on the image and on the physical nature of the signal (in terms, for instance, of its noise statistics), see, e.g., [19] for a review.

In convex scenarios, a common alternative to deal with such methods consists in taking their Fréchet derivative w.r.t. to some norm, which reduces them to evolution equations of the form

$$\frac{\partial}{\partial t} u = -\nabla \mathcal{E}(u), \qquad u|_{t=0} = f, \tag{4}$$

under appropriate conditions on the boundary of the image domain. In this formulation, the solution $u_\star$ in (3) is found alternatively by looking for stationary solutions of the parabolic PDE above. We remark that while the connection between variational problems and parabolic PDEs is always possible by taking the gradient descent, the reverse is not always possible, as it requires some additional structure of the functional space considered that may lack in several cases. We will comment on this issue in the next section, where we will provide some examples in this respect looking at neurophysiologically inspired models for vision.

In such context, evolution equations have been originally used as a tool to describe the physical transmission, diffusion and interaction phenomena of stimuli in the visual cortex, see, e.g. [21]. Similarly, variational methods have been studied by the vision community to describe *efficient neural coding*, see, e.g. [44,35], i.e. all the mechanisms used by the human visual system to *optimise* the visual experience via the reduction of redundant spatio-temporal biases linked to the perceived stimulus.

In the context of vision, a first study on the efficient representation aspects of some neuro-physiological model analogous to the one considered in this work, has been recently performed by the authors in [7] where several visual illusions are tested and reproduced.

2.1 Wilson-Cowan-type models for neuronal activation

A prominent example of evolution models describing neuronal dynamics are the Wilson-Cowan (WC) equations [48,16]. Consider a neuronal population parametrised by a set Ω, endowed with a measure $d\xi$ supported on

the whole Ω. Denoting by $a(\xi,t) \in \mathbb{R}$ the state of a population of neurons with coordinates $\xi \in \Omega$ at time $t > 0$, the Wilson-Cowan model reads

$$\frac{\partial}{\partial t}a(\xi,t) = -\beta a(\xi,t) + \nu \int_\Omega \omega(\xi\|\xi')\sigma(a(\xi',t))\,d\xi' + h(\xi,t). \quad \text{(WC)}$$

Here, $\beta > 0$ and $\nu \in \mathbb{R}$ are fixed parameters, $\omega(\xi\|\xi')$ models interactions at two different locations ξ and ξ', the function h represents an external stimulus, and $\sigma : \mathbb{R} \to \mathbb{R}$ is a non-linear sigmoid saturation function.

In the following we further assume that the interaction kernel ω is non-negative and normalised by

$$\int_\Omega \omega(\xi\|\xi')\,d\xi' = 1. \tag{5}$$

Moreover, as sigmoid σ we consider the following odd function:

$$\sigma(\rho) := \min\{1, \max\{\alpha\rho, -1\}\}, \qquad \alpha > 1, \tag{6}$$

which has been previously considered, e.g., in [9]. Observe that, depending on the sign of ν, model (WC) is able to describe both excitatory ($\nu > 0$) and inhibitory local interactions ($\nu < 0$), see, e.g. [16, Section 3]. Due to the oddness of σ, this latter case can be equivalently expressed by keeping $\nu > 0$ and replacing σ with its "mirrored" version $\hat\sigma(\rho) = \sigma(-\rho), \rho \in \mathbb{R}$, see Figure 2.

Equation (WC) has been studied intensively over the last decades to describe several neuronal mechanisms in V1, see, e.g. , [25,43,21,3,40]. However, one interesting aspect which, up to our knowledge, has not been previously investigated, is whether it complies with any efficient representation principle, or, in more mathematical terms, whether it can be interpreted as the gradient descent of some energy functional in the form (4).

In fact, it is possible to show that the WC model (WC) does not satisfy any variational principle. As a consequence, it cannot implement an efficient neural coding mechanism. A preliminary study has been performed by the authors in a recent preprint [7] in a completely discrete setting. Here, we make these considerations more rigorous by the following theorem.

Theorem 1 *Assume that there exists two sets of positive measure $U_1, U_2 \subset \Omega$, $U_1 \cap U_2 = \varnothing$ such that $\omega(\xi\|\xi') \neq 0$ for any $\xi \in U_1$ and $\xi' \in U_2$. Then, for σ as above, the Wilson-Cowan equation* (WC) *does not admit a variational formulation.*

Proof We proceed by contradiction. Let $\mathcal{E}$ be a densely defined energy functional on $L^2(\Omega)$ such that (WC) can be expressed in the form (4). Let $f_1, f_2 \in L^2(\Omega)$ be two non-negative functions such that

$$\operatorname{supp} f_i \subset U_i, \text{ and } \|f_i\|_{L^2(\Omega)} = 1 \text{ for } i = 1, 2. \tag{7}$$

For any $v \in \mathbb{R}^2$, let us define now $J : \mathbb{R}^2 \to \mathbb{R}$ by

$$J(v) = \mathcal{E}(v_1 f_1 + v_2 f_2). \tag{8}$$

By definition, there holds $\partial_i J(v) = \langle \nabla\mathcal{E}(v_1 f_1 + v_2 f_2), f_i\rangle$, $i = 1, 2$. Thus, by (4) and (WC) we have

$$\partial_i J(v) = \beta v_i - \langle h, f_i\rangle - \nu \int_\Omega\int_\Omega \omega(\xi\|\xi')f_i(\xi)\sigma\left(\sum_{k=1}^2 v_k f_k(\xi')\right) d\xi\,d\xi'. \tag{9}$$

Since σ is Lipschitz by differentiating again we have

$$\partial_{ji} J(v) = \beta\delta_{ij} - \nu \int_{U_j}\left(\int_{U_i} \Psi_{ij}(\xi,\xi')\,d\xi\right)\sigma'\left(v_j f_j(\xi')\right)\,d\xi'. \tag{10}$$

Here, δ_{ij} is the Kroenecker delta symbol. Moreover, we let

$$\Psi_{ij}(\xi,\xi') = \omega(\xi\|\xi')f_i(\xi)f_j(\xi'), \qquad i,j \in \{1,2\}, \tag{11}$$

and observed that, since $\operatorname{supp}\Psi_{ij} \subset \operatorname{supp} f_i \times \operatorname{supp} f_j \subset U_i \times U_j$ and $U_1 \cap U_2 = \varnothing$, it holds

$$\sigma'\left(\sum_{k=1}^2 v_k f_k(\xi')\right) = \sigma'(v_j f_j(\xi')) \qquad \forall \xi' \in U_j. \tag{12}$$

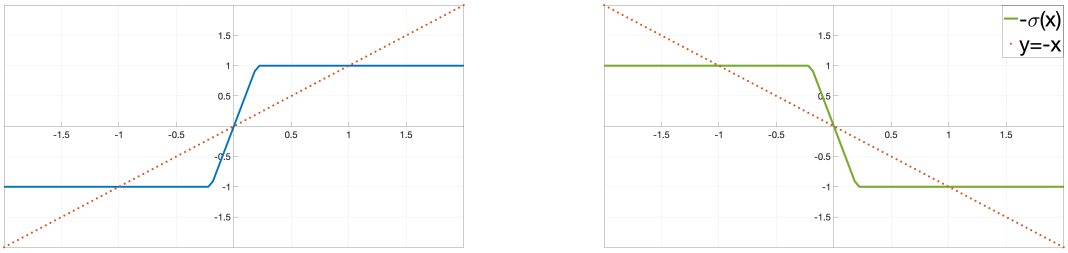
We claim that (10) implies that $J \in C^2$. Indeed, letting m be the measure with density $\int_\Omega \Psi_{ij}(\xi,\cdot)\,d\xi$, explicitly computing σ' yields

$$\partial_{ji} J(v) = \beta\delta_{ij} - \nu\alpha\,\mathrm{m}\left(\{\xi' :\ |f_j(\xi')| \le 1/(\alpha v_j)\}\right). \tag{13}$$

Up to restricting U_1 and U_2, we can assume $\mathrm{m}(\Omega) < +\infty$. Hence, the measurability of f_j and the continuity of the measure m imply that $\partial_{ji}J$ is continuous. This proves the claim.

To conclude the proof, we now show that $\partial_{21}J \not\equiv \partial_{12}J$, which contradicts the C^2 differentiability of J by the Schwarz theorem and thus shows that the r.h.s. of (WC) cannot be the gradient of an energy. To this purpose, let $v \in \mathbb{R}^2$ and compute

$$\begin{aligned}
&\partial_{12}J(v) - \partial_{21}J(v)\\
&= \nu \int_{\Omega\times\Omega}\Big(\Psi_{12}(\xi,\xi')\sigma'\left(v_2 f_2(\xi')\right)\\
&\qquad\qquad - \Psi_{21}(\xi,\xi')\sigma'\left(v_1 f_1(\xi')\right)\Big)\,d\xi\,d\xi'\\
&= \nu \int_{\Omega\times\Omega}\Psi_{12}(\xi,\xi')\left[\sigma'\left(v_2 f_2(\xi')\right) - \sigma'\left(v_1 f_1(\xi)\right)\right]\,d\xi\,d\xi'.
\end{aligned}$$



(a) Excitatory sigmoid σ (b) Inhibitory sigmoid $\widehat{\sigma} = -\sigma$

Fig. 2: Symmetric behaviour of excitatory and inhibitory sigmoid functions in the form (6) with $\alpha = 5$.

(14)

Here, we used that $\Psi_{ji}(\xi, \xi') = \Psi_{ij}(\xi', \xi)$, due to the symmetry of ω. By the explicit expression of σ', letting v_1 tend to infinity and choosing $v_2 = 0$ in the above yields

$$\lim_{v \to (+\infty, 0)} \big(\partial_{12} J(v) - \partial_{21} J(v)\big) = \nu\alpha \int_{\Omega\times\Omega} \Psi_{12}(\xi, \xi')\, d\xi\, d\xi'. \tag{15}$$

The r.h.s. being positive by assumption and by (7), this completes the proof of the statement.

Remark 1 The above argument can be easily extended to any Lipschitz choice of sigmoid σ with non-constant derivative.

To overcome this problem and deal with a model complying with the efficient representation principle, we will consider in the following a variation of (WC) which has been introduced in [9,6,31] for Local Histogram Equalisation (LHE). Using the same notation above, this model can be written as

$$\frac{\partial}{\partial t} a(\xi, t) = -\beta a(\xi, t) + \nu \int_\Omega \omega(\xi \| \xi') \sigma(a(\xi, t) - a(\xi', t))\, d\xi' + h(\xi, t). \tag{LHE}$$

We note that the only difference between (LHE) and (WC) is the different input of the sigmoid σ appearing inside the integral. While in (WC) this is equal to the stimulus intensity at the location ξ', in (LHE), this is equal to a local difference between the population at the point under consideration and a neighbouring one.

Following the same line of proof as in [9], and letting $\Sigma : \mathbb{R} \to \mathbb{R}$ be any (even) primitive function of the sigmoid, it is easy to show that equation (LHE) is in fact the gradient descent in the sense of (4) of the following energy functional

$$\mathcal{E}(a) = \frac{\beta - 1}{2} \int_\Omega |a(\xi)|^2\, d\xi + \frac{1}{2} \int_\Omega |a(\xi) - h(\xi)|^2\, d\xi + \frac{\nu}{2} \int_\Omega \int_\Omega \omega(\xi \| \xi') \Sigma(a(\xi) - a(\xi'))\, d\xi'\, d\xi. \tag{16}$$

2.1.1 Orientation-independent modelling

We now discuss on the application of (LHE) to describe contrast perception phenomena. We model the visual plane as a rectangular domain $Q \subset \mathbb{R}^2$ and consider grey-scale visual stimuli to be functions $f : Q \to [0, 1]$, such that $f(x)$ encodes the brightness intensity at x. In order to derive evolution equations, for a given an initial stimulus f_0 we denote by μ its local intensity average computed as the convolution $\mu = g \star f_0$ of f_0 with some filter $g \in L^1(Q)$ with $\int_Q g(x)\, dx = 1$. Simple Gaussian filters have been considered in [6], whereas a sum of Gaussian filters has been considered in [31] to describe multiple inhibition effects happening at a retinal-level [49]. Note that μ can itself encode a global reference to the Grey-World (GW) principle [9] by simply setting $\mu(x) \equiv 1/2$ for any x. Analogously, we further assume that the activation in (LHE) is given by $a = f - 1/2$ and that the external stimulus h is given by a weighted sum of the initial stimulus $a|_{t=0} = f_0 - 1/2$ and its filtering via g. Namely, for $\lambda > 0$,

$$h = (g \star a)|_{t=0} + \lambda a|_{t=0} = \mu + \lambda f_0 - \frac{1 + \lambda}{2}. \tag{17}$$

By simply plugging these ingredients in (LHE), and letting $\beta = 1 + \lambda$, we obtain the following (orientation-independent) LHE evolution model:

$$\frac{\partial}{\partial t} f(x, t) = -(1 + \lambda) f(x, t) + \nu \int_Q \omega(x, y) \sigma\big(f(x, t) - f(y, t)\big)\, dy + (\mu(x) + \lambda f_0(x)). \tag{LHE-2D}$$

We stress that our particular choice of β is motivated again by the GW principle. In fact, one can check that this is the only choice guaranteeing that the constant visual stimulus $f_0(x) \equiv 1/2$ is indeed a fixed point for this evolution model.

As far as the interaction kernel ω is concerned, in [31] the authors consider in (LHE) a kernel ω which is a convex combination of two bi-dimensional Gaussians with different standard deviations. While this variation of the model (LHE-2D) is effective in describing *assimilation* effects, the lack of dependence on the local orientation makes such modelling intrinsically not adapted to explain orientation-induced contrast and colour perception effects such as the ones described in [36,41,12]. Reference models capable to explain these effects are mostly based on oriented Difference of Gaussian linear filtering coupled with some non-linear processing, such as the ODOG and the BIWaM models described in [12, 11] and [36], respectively. However, despite their good effectiveness in the description of several visual perception phenomena, these are not based on any neuronal evolution modelling nor on any efficient representation principle.

2.1.2 Orientation-dependent modelling

Let us turn to the orientation-dependent models. For a given visual stimulus f, we let $Lf : Q \times [0,\pi) \to \mathbb{R}$ be the corresponding cortical activation in V1, where $Lf(x,\theta)$ encodes the response of the neuron with spatial preference x and orientation preference θ to the stimulus f. Such activation is obtained via convolution with the receptive fields of V1 neurons, as explained in Appendix A, see also [37,20,24,38]. Then, similarly to above, we consider $a = F - 1/2$ for $F(x,\theta)$, and take as external stimulus $h = L\mu + \lambda Lf_0 - (1+\lambda)/2$. This, and the choice $\beta = 1+\lambda$, yield to the equation

$$\begin{aligned}\frac{\partial}{\partial t}F(x,\theta,t) &= -(1+\lambda)F(x,\theta,t) \qquad \text{(LHE-3D)}\\ &+ \nu\int_0^\pi\int_Q \omega(x,\theta\|y,\phi)\sigma\big(F(x,\theta,t) - F(y,\phi,t)\big)\,dy\,d\phi\\ &+ \left(L\mu(x,\theta) + \lambda Lf_0(x,\theta)\right).\end{aligned}$$

We remark once again that the above model describes the dynamic behaviour of activations in the 3D space of positions and orientation. As explained in Appendix A, once a stationary solution is found, the two-dimensional perceived image can be efficiently found by

$$f(x) = \frac{1}{\pi}\int_0^\pi F(x,\theta)\,d\theta. \tag{18}$$

Remark 2 In the following we will consider the interaction to be excitatory (i.e., $\nu > 0$) for both (LHE-2D) and (LHE-3D) models. Indeed, the integral term in both models is positive at x if, e.g., $f(x,t) > f(y,t)$. Thus, in order to enhance the contrast between x and its surround we need to have $\nu > 0$.

We now discuss on the numerical aspects required to implement model (LHE-3D).

2.2 Discretisation via gradient descent

First, we discretise the initial (square) image f_0 as an $N \times N$ matrix. For simplicity, here we assume periodic boundary conditions. We additionally consider $K \in \mathbb{N}$ orientations, parametrised by $k \in \{1,\dots,K\} \mapsto \theta_k := (k-1)\pi/K$.

The discretised lift operator, still denoted by L, then transforms $N \times N$ matrices into $N \times N \times K$ arrays. Its action on an $N \times N$ matrix f is defined for $n,m \in \{1,\dots,N\}$ and $k \in \{1,\dots,K\}$ by

$$(Lf)_{n,m,k} = \mathcal{F}^{-1}\left((\mathcal{F}f) \odot (R_{\theta_k}\mathcal{F}\Psi^{\text{cake}})\right)_{n,m}, \tag{19}$$

where $\odot$ is the Hadamard (i.e., element-wise) product of matrices, $\mathcal{F}$ denotes the discrete Fourier transform, R_{θ_k} is the rotation of angle θ_k, and Ψ^{cake} is the cake mother wavelet (see Appendix A).

We let $F^0 = Lf_0$, and $G_0 = L\mu$, where the local intensity average μ is given by a Gaussian filtering of f_0. The explicit time-discretisation of the gradient descent (LHE-3D) is, for $\Delta t \ll 1$ and $\ell \in \mathbb{N}$,

$$\frac{F^{\ell+1} - F^\ell}{\Delta t} = -(1+\lambda)F^\ell + G_0 + \lambda F^0 + \frac{1}{2M}R_{F^\ell}. \tag{20}$$

Here, for a given 3D Gaussian matrix W encoding the weight ω, and an $N \times N \times M$ matrix F, we let, for any $n,m \in \{1,\dots,N\}$ and $k \in \{1,\dots,K\}$,

$$\begin{aligned}&(R_F)_{n,m,k}\\ &:= \sum_{n',m'=1}^{N}\sum_{k'=1}^{K} W_{n-n',m-m',k-k'}\sigma(F_{n,m,k} - F_{n',m',k'}).\end{aligned} \tag{21}$$

We refer to [9, Section IV.A] for the description of an efficient numerical approach used to compute the above quantity in the 2D case and that can be translated verbatim to the 3D case under consideration.

After a suitable number of iterations $\bar{\ell}$ of the above algorithm (measured by the stopping criterion $\|F^{\ell+1} - F^\ell\|_2/\|F^\ell\|_2 \le \tau$, for a fixed tolerance $\tau \ll 1$), the output image is then found via (18) as $\bar{f}_{n,m} = \sum_{k=1}^{K} F^{\bar{\ell}}_{n,m,k}$.

3 Numerical results

In this section we present the results obtained by applying the cortical-inspired model presented in the previous section to some well-known phenomena where contrast perception may be affected by local orientations.

We compare the results obtained by our orientation-dependent 3D model (LHE-3D) with the corresponding 2D model (LHE-2D) already considered in [31,6] for histogram equalisation and contrast enhancement. We further compare the performance of these models with two standard reference models based on oriented Gaussian filtering: the Oriented Difference Of Gaussians (ODOG) model [12], and the Brightness Induction Wavelet Model (BIWaM), introduced in [36]. In the former, the output is computed via a convolution of the input image with oriented difference of Gaussian filters in six orientations and seven spatial frequencies. The filtering outputs within the same orientation are then summed in a non-linear fashion privileging higher frequencies. The BIWaM model is then a variation of the ODOG one, the difference being the dependence on the local surround orientation of the contrast sensitivity function[1].

Parameters. All the images considered in the following numerical experiments have size 200×200 pixels. The lifting procedure to the space of positions and orientations is by discretising $[0, \pi]$ via $K = 30$ orientations. The relevant cake wavelets are then computed following [5], setting the frequency band `bw` to `bw` $= 4$ for all experiments. In (LHE-3D), we compute the local mean average μ and the integral term by Gaussian filtering with standard deviation σ_μ and σ_ω, respectively. The gradient descent algorithm stops when the relative stopping criterion defined in Section 2.2 is verified with a tolerance $\tau = 10^{-2}$.

3.1 Non-orientation-dependent examples

In this section we test (LHE-2D) and (LHE-3D) on several classical non-orientation-dependent illusions. In particular, we focus on the three following examples: (i) *White's illusion* [47], presented in Figure 3a. Here, the left gray rectangle appears darker than the right one, although both are identical. (ii) The *Simultaneous Brightness Contrast* [17], presented in Figure 3b, consists in the lighter appearance of the left gray square than the right one, while both are identical. (iii) The *Luminance illusion* [32] presented in Figure 3c, consists in four identical dots over a background where intensity increases from left to right: the dots on the left are perceived being lighter than the ones on the right.
See [7] for more non-orientation-dependent examples.

Discussion. As Figure 3 shows, both (LHE-2D) and (LHE-3D) are predicting the three described illusions. Notice that also the BIWaM and ODOG methods can correctly reproduce them (see, e.g., [12,36]).

3.2 Grating induction with oriented background

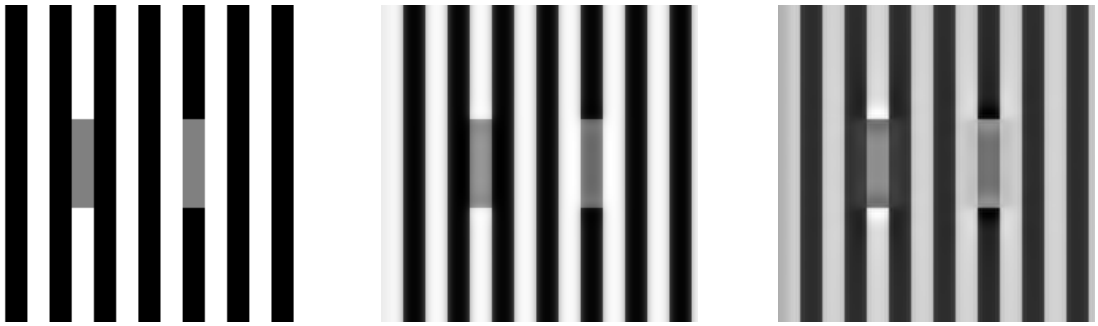
Grating induction (GI) is a contrast effect which has been first described in [34] and later studied, e.g., in [12]. As the name suggests, the phenomenon describes the induction of a regular alternation of intensity changes on a constant image region due to the presence of an inducing background.

In this section we describe our results on a variation of GI where a relative orientation θ describes how much the background is oriented with respect to a constant gray bar in the middle of the image, see Figure 4. Here, when the background has a different orientation from the central grey bar (i.e. $\theta > 0$), an alternation of dark-grey/light-grey patterns within the central bar, is produced and perceived by the observer. This phenomenon is contrast dependent, as the intensity of the induced grey patterns (dark-grey/light-grey) is in opposition with the background grating. Moreover, it is also orientation-dependent, since the perceived intensity of the phenomenon varies depending on the background orientation, and, in particular, it is maximal when the background bars are orthogonal to the central one.

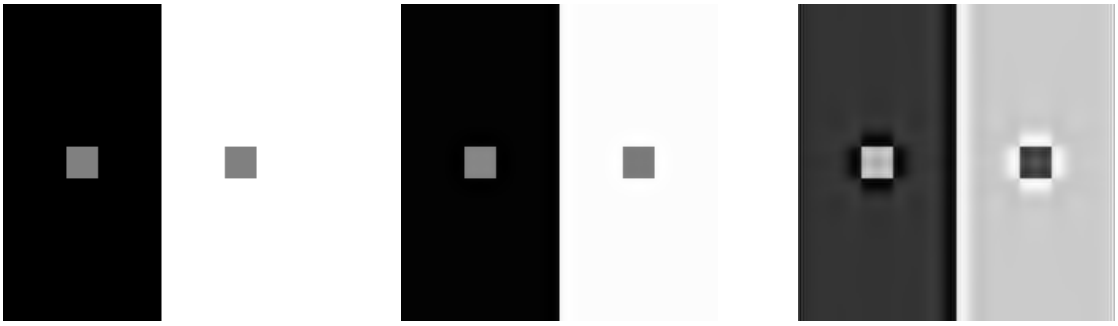
Discussion. We observe that, in accordance with visual perception, model (LHE-3D) predicts the appearance of a counter-phase grating in the central grey bar, see Figures 5d and 7d. The same result is obtained by the ODOG model, see Figures 5a and 7a. In particular, Figures 6 and 8 show higher intensity profile when the background gratings are orthogonal to the central line, with respect to the case of background angle equal to $\pi/3$, see orange and green dashed line. On the other hand, BIWaM and (LHE-2D) models do not appear suitable to describe this phenomenon. See for comparison the red and blue dashed lines in Figures 6 and 8.

We will now consider a similar example, focusing more precisely on the illusory completion of collinear lines of the background in correspondence of the central gray bar.

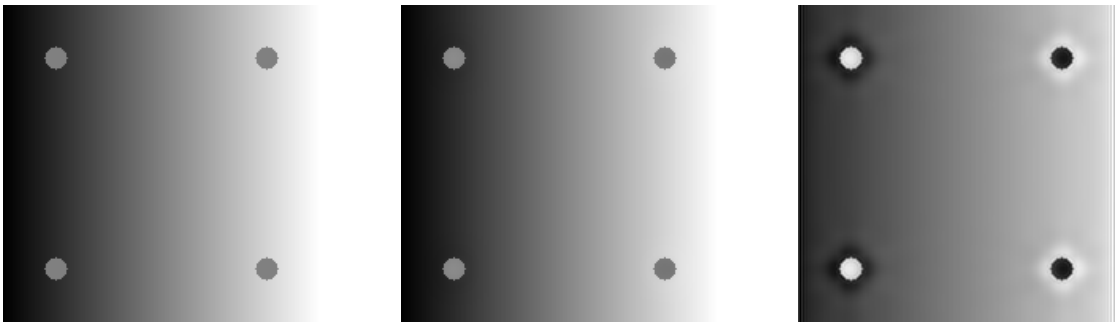
[1] For our comparisons we used the ODOG and BIWaM codes freely available at https://github.com/TUBvision/betz2015_noise.



(a) White's illusion.



(b) Simultaneous Brightness Contrast illusion.



(c) Luminance illusion.

Fig. 3: Reconstruction of non-orientation-dependent examples. *First column:* Original image. *Second column:* Reconstruction via the (LHE-2D) model. *Third column:* Reconstruction via the (LHE-3D) model. Parameters for (LHE-3D): $\sigma_\mu = 3$, $\sigma_\omega = 8$, $\lambda = 0.5$.

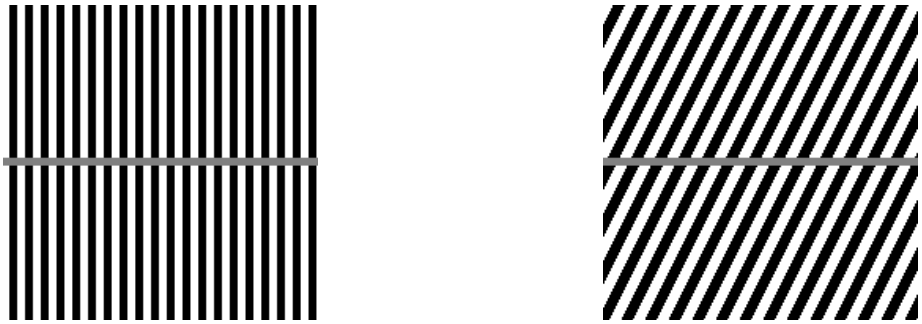
3.3 Poggendorff illusion

The Poggendorff illusion (see Figure 9b) consists in the perceived misalignment of two segments of a same continuous line due to the presence of a superposed surface. The perceived perceptual bias of the phenomenon has been investigated and studied via neurophysiological experiments, see, e.g., [45,46]. Recently, in [26,27], a sub-Riemannian framework where orientations are computed via Gabor filters has been used to study the geometrical VS. perceptual completion effects induced by the illusion, successfully mimicking our perception. Here, we consider a modified version of the Poggendorff illusion, where the background is constituted by a grating pattern, see Figure 9a, in order to account for both contrast and orientation features.

Note that this example is actually similar to the one considered in the previous section, the only difference being the width of the central grey bar, which is the responsible of the perceived misalignment.

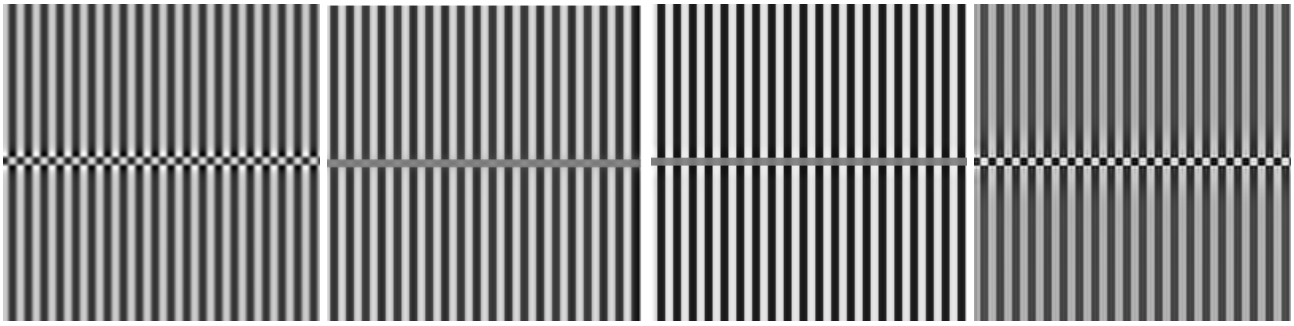
Discussion. The result obtained by applying (LHE-3D) to Figure 9a is presented in Figures 9c and 10d. As for the results on the grating induction presented in Section 3.2, we observe an induced counter-phase grating in the central grey bar.

In this experiment we focus on whether it is possible to compute numerically an image output reproducing



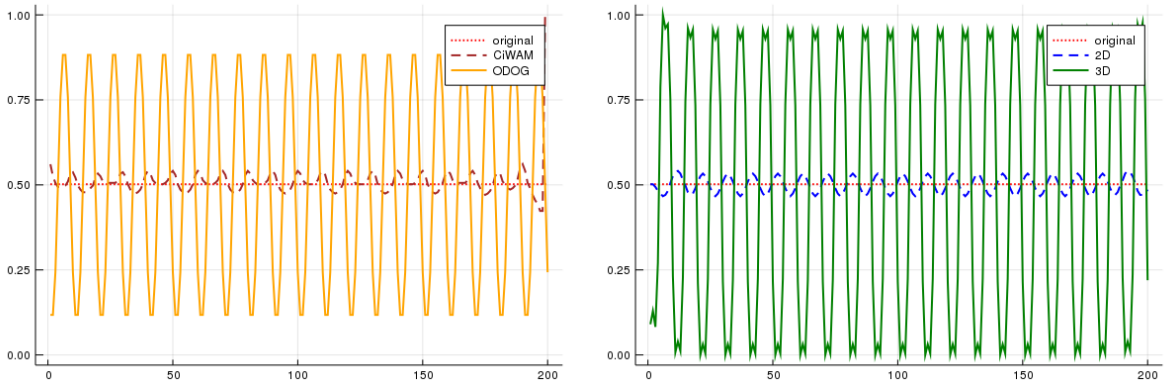
(a) Relative orientation $\theta = \pi/2$. (b) Relative orientation $\theta = \pi/3$.

Fig. 4: Grating inductions with varying background orientation.



(a) ODOG. (b) BIWaM. (c) (LHE-2D). (d) (LHE-3D).

Fig. 5: Model outputs of input Fig. 4a. Parameters for (d): $\sigma_\mu = 10$, $\sigma_\omega = 5$, $\lambda = 0.5$.

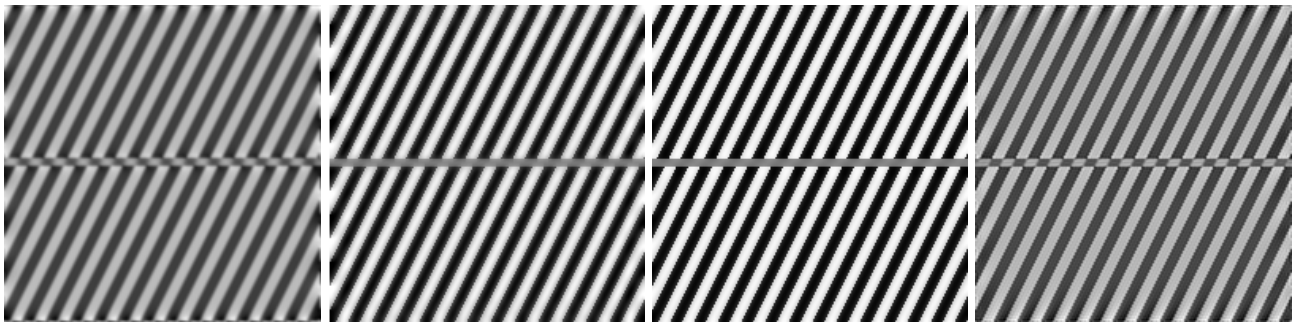


(a) ODOG and BIWaM. (b) (LHE-2D) VS (LHE-3D) models.

Fig. 6: Middle line-profiles of outputs in Fig. 5.

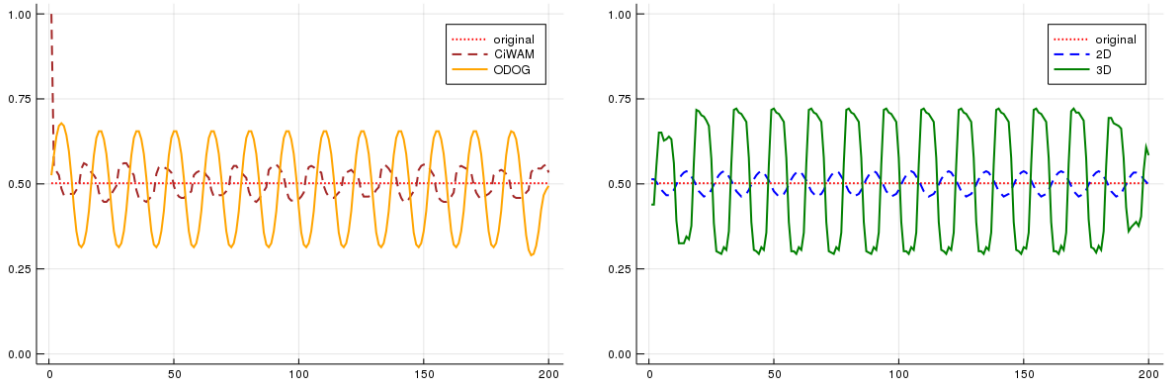
the perceived misalignment between some fixed black stripe in the bottom part of Figure 9a and its collinear prosecution in the upper part. Note that the perceived alignment differs from the actual geometrical one: for a fixed black stripe in the bottom part, the alignment of the corresponding collinear top stripe is in fact perceived slightly flushed left, see Figure 9b, where single stripes have been isolated for better visualisation. The problem here is therefore not an inpainting problem, which is classical in the imaging community, but is rather to reconstruct the perceptual output from the given input in Fig. 9a.

We now look at the results in Figure 9c and mark by a continuous green line a fixed black stripe in the bottom part of the image. In order to find the corresponding perceived collinear stripe in the upper part, we follow how the model propagates the marked stripe across the central surface (dashed green line). We notice that the prosecution computed via the (LHE-3D) model does not correspond to its actual collinear prose-



(a) ODOG. (b) BIWaM. (c) (LHE-2D). (d) (LHE-3D).

Fig. 7: Model outputs of input in Fig. 4b. Parameters for (d): $\sigma_\mu = 10$, $\sigma_\omega = 5$, $\lambda = 0.5$.



(a) ODOG and BIWaM. (b) (LHE-2D) VS(LHE-3D) models.

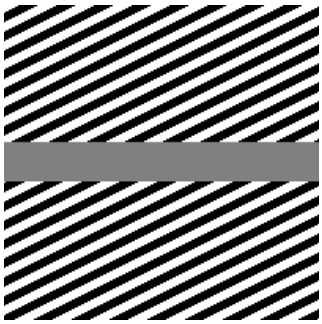
Fig. 8: Middle line-profiles of outputs in Figure 7.

cution, but, rather, it is in agreement with our perception. Comparisons with reference models are presented in Figures 10 and 11. We observe that the results obtained via the proposed (LHE-3D) model cannot be reproduced by the BIWaM nor the (LHE-2D) models, which moreover induce a non-counter-phase grating in the central grey bar which is different from the expected perceptual result. On the other hand, the result obtained by the ODOG model is consistent with ours, but presents a much less evident alternating grating within the central grey bar. In particular, the induced oblique bands are not visibly connected across the whole grey bar, i.e. their induced contrast is very poor and, consequently, the induced edges are not as sharp as the ones reconstructed via our model, see Figure 11 for an example on the middle-line profile.

We stress that a numerical implementation of the standard (WC) model, whose result is presented in Figure 13, is not able to reproduce the desired perceptual completion. We believe such failure in replicating the illusion to be due to the lack of a variational efficient representation as shown in Theorem 1.

Threshold for inpainting versus perceptual completion in the grating Poggendorff. Interestingly, the capability of model (LHE-3D) to reproduce the visual phenomenon is very much dependent on the choice of the parameters σ_ω, which accounts for the interaction among different hypercolumns of the visual cortex, i.e. simple cells that refer to the same portion of the retina, see Figure 14. As pointed out by the seminal works of Hubel, Wiesel and Bosking [30,42,15], it is possible in fact to identify at least two main types of connectivity in the visual cortex: the intra-cortical connectivity, able to select the preferred orientations among cells belonging to the same hypercolumn and the long-range connectivity, connecting simple cells belonging to different hypercolumns.

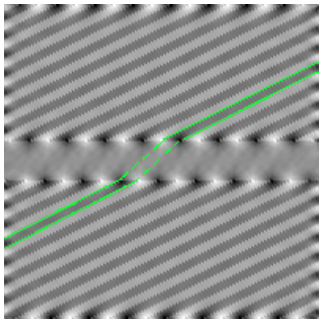
Perceptual phenomena such as those presented in this work arise by means of an interaction between these two connectivities, modelled in (LHE-3D) by the parameter σ_ω, that is, the standard variation of the Gaussian ω, therefore accounting for smaller or bigger local interactions. This parameter can thus be modulated to simulate different type of interactions between different hypercolumns: when σ_ω is small with respect to the overall size of the processed image, the geomet-



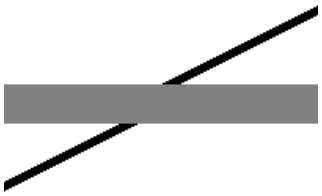
(a) A variation of the Poggendorff illusion. The presence of the grey central surface induces a misalignment of the background lines.



(b) The classical Poggendorff illusion, extracted from Fig. 9a.



(c) Output of model (LHE-3D).



(d) The extracted perceived alignment computed.

Fig. 9: Poggendorff illusion: input and result by (LHE-3D). Parameters: $\sigma_\mu = 3$, $\sigma_\omega = 10$, $\lambda = 0.5$.

rical completion (inpainting) can be reproduced. When it is bigger, perceptual-oriented phenomena such as illusory contours or geometrical optical illusions can be modelled. The gradual change between these two types of interactions depending on the size of ω is shown in Figure 12, which highlights also the flexibility of our approach when it comes both to image processing and to the modelling of the neural activity in the visual cortex.

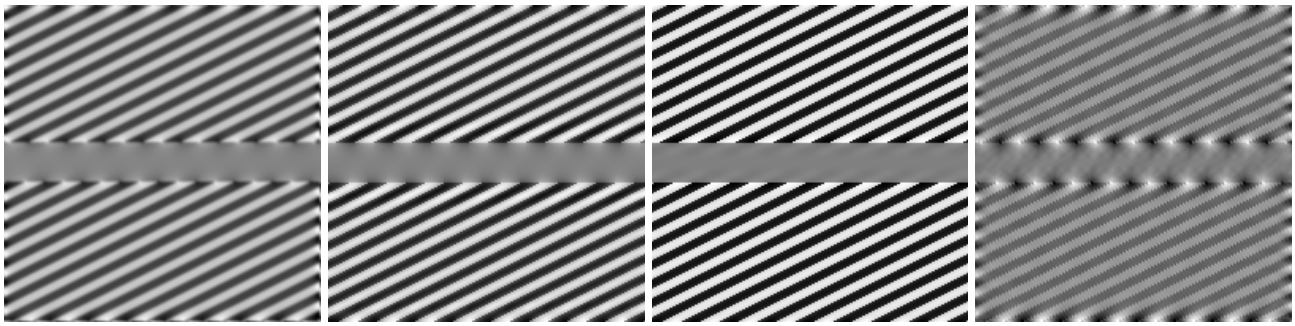
4 Conclusions

In this paper, we considered a neuro-physiological evolution model to study visual perception bias due to contrast and, possibly, to local orientation dependence. The proposed model has been originally introduced in [9] in the context of image processing for local histogram equalisation (LHE) and is a variation of the celebrated Wilson and Cowan (WC) equations (1), formulated in [48] to describe the evolution of a population of neurons in V1.

Firstly, in Section 2 we investigated on the efficient representation properties of the original WC model in contrast to the LHE one. In mathematical terms this consists in interpreting the corresponding dynamics as the gradient descent of suitable energy functionals. We rigorously proved that for the WC model there is no energy minimised by the WC-dynamics (Theorem 1), while for the LHE variant, there exists an energy functional (see formula (16)) minimised by its stationary solutions.

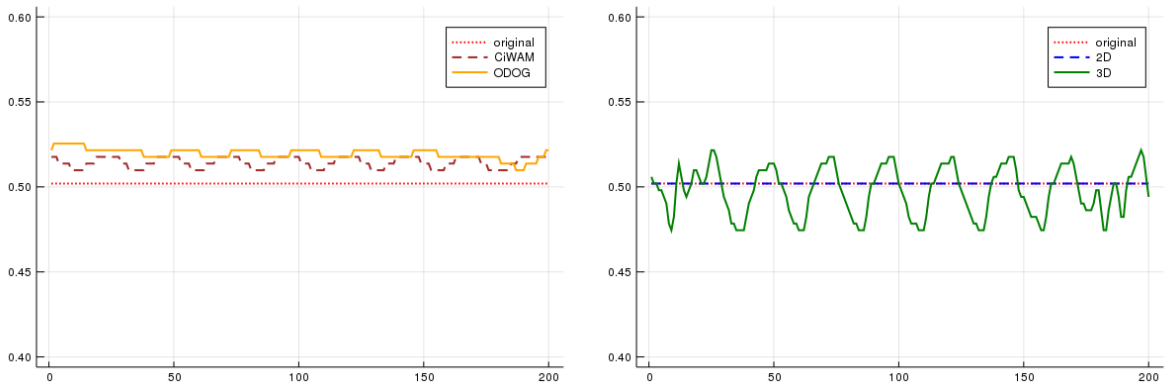
Secondly, by mimicking the structure of V1, we extended the mathematical formulation of the LHE model to a third dimension in order to describe local orientation preference. This new model, denoted by (LHE-3D), can be efficiently implemented via convolution with appropriate kernels and solved numerically via standard explicit schemes. The information on the local orientation allows to describe contrast phenomena as well as orientation-dependent illusions.

In Section 3 we tested this extension of LHE for some orientation-independent brightness illusions, showing that it is able to reproduce the perceptual results as well as standard Linear + Non-Linear filtering (such as the ODOG and the BIWaM models [12,36]) can do. Then, we performed some further test on orientation-dependent illusions (such as grating induction and the Poggendorff illusion), observing that only the proposed orientation-dependent extension of the LHE model is capable to replicate the perceived visual bias. In agreement with the theoretical sub-optimality of the standard WC model with respect to the efficient representation principle pointed out before, it turns out that



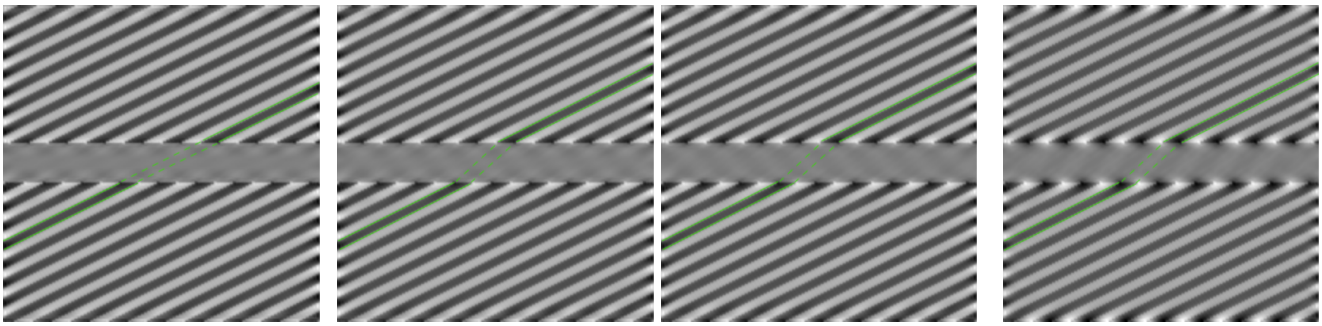
(a) ODOG. (b) BIWaM. (c) (LHE-2D). (d) (LHE-3D).

Fig. 10: Reconstruction of the Poggendorff illusion 9a via reference models.



(a) ODOG and BIWaM. (b) (LHE-2D) VS (LHE-3D) models.

Fig. 11: Middle line-profiles of outputs in Figure 10.



(a) $\sigma_\omega = 5$ (b) $\sigma_\omega = 6$ (c) $\sigma_\omega = 7$ (d) $\sigma_\omega = 10$

Fig. 12: Sensitivity to parameter σ_w for (LHE-3D) model. The completion inside the middle gray bar changes from geometrical (inpainting-type) to illusory (perception-type). Fixed parameters: $\sigma_\mu = 2$, $\lambda = 0.8$.

(LHE-3D) is the only model capable of replicating the illusion.

Finally, we reported a preliminary empirical discussion on the sensitivity of model (LHE-3D) to parameters describing different connectivity properties between hypercolumns in V1. Our experiment revealed the existence of a threshold parameter in correspondence of which the completion properties of model (LHE-3D) switch from inpainting-type to perceptual-type. A more accurate theoretical study based, e.g., on bifurcation and stability analysis of the equilibria of the model, is left for future research.

Further investigations should also address a more accurate modelling reflecting the actual structure of V1. In particular, this concerns the lift operation where the cake wavelet filters should be replaced by Gabor filtering as in [27], as well as the interaction weight ω which could be taken to be the anisotropic heat kernel of [20].

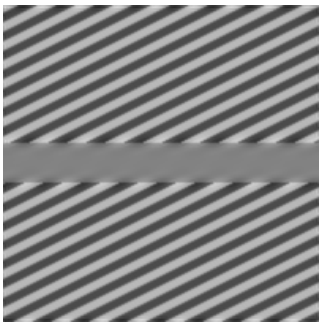


Fig. 13: Model output of the standard (WC) model for the input in Fig. 9a. See [7] for other results via the (WC) models and details on the implementation.

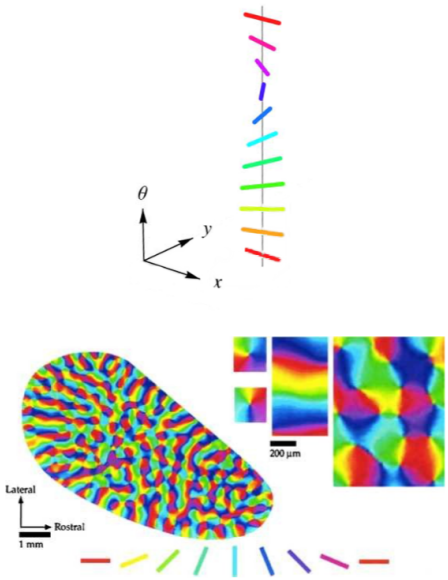


Fig. 14: In this image we illustrate the difference between intra-cortical connectivity (top) and long range one (bottom), respectively from [20] and [15].

Finally, extensive numerical experiments should be performed to assess the compatibility of the model with psycho-physical tests measuring the perceptual bias induced by these and other phenomena such as the ones discussed in [7]. This would provide insights about the robustness of the model in reproducing the visual pathway behaviour.

A Orientation-dependent model of V1

Let us denote by $R > 0$ the size of the visual plane and let $D_R \subset \mathbb{R}^2$ be the disk $D_R := \{x_1^2 + x_2^2 \leq R^2\}$. Fix $R > 0$ such that $Q \subset D_R$. In order to exploit the properties of the roto-translation group $SE(2)$ on images, we now consider them to be elements of the set:

$$\mathcal{I} = \left\{ f \in L^2(\mathbb{R}^2, [0,1]) \text{ such that } \operatorname{supp} f \subset D_R \right\}. \quad (22)$$

We remark that fixing $R > 0$ is necessary, since contrast perception is strongly dependent on the scale of the features under consideration w.r.t. the visual plane.

Orientation dependence of the visual stimulus is encoded via cortical inspired techniques, following e.g., [37,20,24,38,13]. The main idea at the base of these works goes back to the 1959 paper [30] by Hubel and Wiesel (Nobel prize in 1981) who discovered the so-called *hypercolumn functional architecture* of the visual cortex V1.

Each neuron ξ in V1 is assumed to be associated with a receptive field (RF) $\psi_\xi \in L^2(\mathbb{R}^2)$ such that its response under a visual stimulus $f \in \mathcal{I}$ is given by

$$F(\xi) = \langle \psi_\xi, f \rangle_{L^2(\mathbb{R}^2)} = \int_{\mathbb{R}^2} \overline{\psi_\xi(x)} f(x)\, dx. \quad (23)$$

Since each neuron is sensible to a preferred position and orientation in the visual plane, we let $\xi = (x, \theta) \in \mathcal{M} = \mathbb{R}^2 \times \mathbb{P}^1$. Here, $\mathbb{P}^1$ is the projective line that we represent as $[0, \pi]/\sim$, with $0 \sim \pi$. Moreover, in order to respect the *shift-twist* symmetry [16, Section 4], we will assume that the RF of different neurons are "deducible" one from the other via a linear transformation. Let us explain this in detail.

The double covering of $\mathcal{M}$ is given by the Euclidean motion group $SE(2) = \mathbb{R}^2 \rtimes \mathbb{S}^1$, that we consider endowed with its natural semi-direct product structure. That is, for $(x, \theta), (y, \varphi) \in SE(2)$, we let

$$(x, \theta) \star (y, \varphi) = (x + R_\theta y, \theta + \varphi), \quad (24)$$

$$\text{where } R_\theta = \begin{pmatrix} \cos\theta & -\sin\theta \\ \sin\theta & \cos\theta \end{pmatrix}. \quad (25)$$

In particular, the above operation induces an action of $SE(2)$ on $\mathcal{M}$, which is thus an homogeneous space. Observe that $SE(2)$ is unimodular and that its Haar measure (the left and right-invariant measure up to scalar multiples) is $dxd\theta$.

We now denote by $\mathcal{U}(L^2(\mathbb{R}^2)) \subset \mathcal{L}(L^2(\mathbb{R}^2))$ the space of linear unitary operators on $L^2(\mathbb{R}^2)$ and let $\pi : SE(2) \to \mathcal{U}(L^2(\mathbb{R}^2))$ be the *quasi-regular representation* of $SE(2)$. That is, $\pi(x, \theta) \in \mathcal{U}(L^2(\mathbb{R}^2))$ is the unitary operator encoding the action of the roto-translation $(x, \theta) \in SE(2)$ on square-integrable functions on $\mathbb{R}^2$. The action of $\pi(x, \theta)$ on $\psi \in L^2(\mathbb{R}^2)$ is

$$[\pi(x, \theta)\psi](y) = \psi((x, \theta)^{-1} y) = \psi(R_{-\theta}(y - x)), \quad \forall y \in \mathbb{R}^2.$$

Moreover, we let $\Lambda : SE(2) \to \mathcal{U}(L^2(SE(2)))$ be the *left-regular representation*, which acts on functions $F \in L^2(SE(2))$ as

$$[\Lambda(x,\theta)F](y,\varphi) = F((x,\theta)^{-1} \star (y,\varphi)),\ \forall (y,\theta) \in SE(2). \tag{26}$$

Letting $L : L^2(\mathbb{R}^2) \to L^2(\mathcal{M})$ be the operator that transforms visual stimuli into cortical activations, one can formalise the *shift-twist* symmetry by requiring

$$L \circ \pi(x,\theta) = \Lambda(x,\theta) \circ L, \qquad \forall (x,\theta) \in SE(2). \tag{27}$$

Under mild continuity assumption on L, it has been shown in [38] that L is then a continuous wavelet transform. That is, there exists a *mother wavelet* $\Psi \in L^2(\mathbb{R}^2)$ satisfying $\pi(x,\theta)\Psi = \pi(x,\theta+\pi)\Psi$ for all $(x,\theta) \in SE(2)$, and such that

$$Lf(x,\theta) = \langle \pi(x,\theta)\Psi, f\rangle, \quad \forall f \in L^2(\mathbb{R}^2), (x,\theta) \in \mathcal{M}. \tag{28}$$

Observe that the operation $\pi(x,\theta)\Psi$ above is well defined for $(x,\theta) \in \mathcal{M}$ thanks to the assumption on Ψ. By (23), the above representation of L is equivalent to the fact that the RF associated with the neuron $(x,\theta) \in \mathcal{M}$ is the roto-translation of the mother wavelet, i.e., $\psi_{(x,\theta)} = \pi(x,\theta)\Psi$.

Remark 3 Letting $\Psi^*(x) := \overline{\Psi(-x)}$, the above formula can be rewritten as

$$\begin{aligned} Lf(x,\theta) &= \int_{\mathbb{R}^2} \overline{\Psi(R_{-\theta}(y-x))} f(y)\, dy \\ &= \big[f * (\Psi^* \circ R_{-\theta})\big](x), \quad \forall (x,\theta) \in SE(2). \end{aligned} \tag{29}$$

where $f * g$ denotes the standard convolution on $L^2(\mathbb{R}^2)$.

Neuro-physiological evidence shows that a good fit for the RFs is given by Gabor filters, whose Fourier transform is simply the product of a Gaussian with an oriented plane wave [22]. However, these filters are quite challenging to invert, and are parametrised on a bigger space than $\mathcal{M}$, which takes into account also the frequency of the plane wave and not only its orientation. For this reason, in this work we chose to consider as wavelets the *cake wavelets* introduced in [23], see also [5]. These are obtained via a mother wavelet Ψ^{cake} whose support in the Fourier domain is concentrated on a fixed slice, which depends on the number of orientations one aims to consider in the numerical implementation. To recover integrability properties, the Fourier transform of this mother wavelet is then smoothly cut off via a low-pass filtering, see [5, Section 2.3] for details. Observe, however, that in order to lift to $\mathcal{M}$ and not to $SE(2)$, we consider a non-oriented version of the mother wavelet, given by $\tilde{\psi}^{cake}(\omega) + \tilde{\psi}^{cake}(e^{i\pi}\omega)$, in the notations of [5].

An important feature of cake wavelets is that, in order to recover the original image, it suffices to consider the *projection operator* defined by

$$P : L^2(\mathcal{M}) \to L^2(\mathbb{R}^2), \tag{30}$$

$$PF(x) := \int_{\mathbb{P}^1} F(x,\theta)\, d\theta, \qquad F \in L^2(\mathcal{M}) \tag{31}$$

Indeed, by construction of cake wavelets, Fubini's Theorem shows that $(P \circ L)f = f$ for all $f \in \mathcal{I}$.

References

1. Atick, J.J.: Could information theory provide an ecological theory of sensory processing? Network: Computation in neural systems **3**(2), 213–251 (1992)
2. Attneave, F.: Some informational aspects of visual perception. Psychological review **61**(3), 183 (1954)
3. Barbieri, D., Citti, G., Cocci, G., Sarti, A.: A cortical-inspired geometry for contour perception and motion integration. J. Math. Imaging Vis. **49**(3), 511–529 (2014). DOI 10.1007/s10851-013-0482-z
4. Barlow, H.B., et al.: Possible principles underlying the transformation of sensory messages. Sensory communication **1**, 217–234 (1961)
5. Bekkers, E., Duits, R., Berendschot, T., ter Haar Romeny, B.: A multi-orientation analysis approach to retinal vessel tracking. Journal of Mathematical Imaging and Vision **49**(3), 583–610 (2014)
6. Bertalmío, M.: From image processing to computational neuroscience: a neural model based on histogram equalization. Frontiers in Computational Neuroscience **8**, 71 (2014)
7. Bertalmío, M., Calatroni, L., Franceschi, V., Franceschiello, B., Gomez-Villa, A., Prandi, D.: Visual illusions via neural dynamics: Wilson-Cowan-type models and the efficient representation principle (2019). ArXiv preprint: https://arxiv.org/abs/1907.13004
8. Bertalmío, M., Calatroni, L., Franceschi, V., Franceschiello, B., Prandi, D.: A cortical-inspired model for orientation-dependent contrast perception: A link with wilson-Cowan equations. In: J. Lellmann, M. Burger, J. Modersitzki (eds.) Scale Space and Variational Methods in Computer Vision, pp. 472–484. Springer International Publishing, Cham (2019)
9. Bertalmío, M., Caselles, V., Provenzi, E., Rizzi, A.: Perceptual color correction through variational techniques. IEEE Transactions on Image Processing **16**(4), 1058–1072 (2007)
10. Bertalmío, M., Cowan, J.D.: Implementing the retinex algorithm with Wilson-Cowan equations. Journal of Physiology-Paris **103**(1), 69 – 72 (2009)
11. Blakeslee, B., Cope, D., McCourt, M.E.: The oriented difference of gaussians (ODOG) model of brightness perception: Overview and executable *Mathematica* notebooks. Behavior Research Methods **48**(1), 306–312 (2016)

12. Blakeslee, B., McCourt, M.E.: A multiscale spatial filtering account of the White effect, simultaneous brightness contrast and grating induction. Vision Research **39**(26), 4361 – 4377 (1999)
13. Bohi, A., Prandi, D., Guis, V., Bouchara, F., Gauthier, J.P.: Fourier descriptors based on the structure of the human primary visual cortex with applications to object recognition. Journal of Mathematical Imaging and Vision **57**(1), 117–133 (2017). DOI 10.1007/s10851-016-0669-1
14. Boscain, U.V., Chertovskih, R., Gauthier, J.P., Prandi, D., Remizov, A.: Highly corrupted image inpainting through hypoelliptic diffusion. Journal of Mathematical Imaging and Vision **60**(8), 1231–1245 (2018). DOI 10.1007/s10851-018-0810-4
15. Bosking, W.H., Zhang, Y., Schofield, B., Fitzpatrick, D.: Orientation selectivity and the arrangement of horizontal connections in tree shrew striate cortex. Journal of neuroscience **17**(6), 2112–2127 (1997)
16. Bressloff, P.C., Cowan, J.D.: An amplitude equation approach to contextual effects in visual cortex. Neural Computation **14**(3), 493–525 (2002)
17. Brucke, E.: uber erganzungs und contrasfarben. Wiener Sitzungsber **51** (1865)
18. Carandini, M., Demb, J.B., Mante, V., Tolhurst, D.J., Dan, Y., Olshausen, B.A., Gallant, J.L., Rust, N.C.: Do we know what the early visual system does? Journal of Neuroscience **25**(46), 10577–10597 (2005)
19. Chan, T., Shen, J.: Image Processing and Analysis. Society for Industrial and Applied Mathematics (2005). DOI 10.1137/1.9780898717877
20. Citti, G., Sarti, A.: A cortical based model of perceptual completion in the roto-translation space. Journal of Mathematical Imaging and Vision **24**(3), 307–326 (2006)
21. Cowan, J.D., Neuman, J., van Drongelen, W.: Wilson–cowan equations for neocortical dynamics. The Journal of Mathematical Neuroscience **6**(1), 1 (2016)
22. Daugman, J.G.: Uncertainty relation for resolution in space, spatial frequency, and orientation optimized by two-dimensional visual cortical filters. Journal of the Optical Society of America. A, Optics and image science **2**(7), 1160–1169 (1985)
23. Duits, R., Felsberg, M., Granlund, G., Haar Romenij, ter, B.: Image analysis and reconstruction using a wavelet transform constructed from a reducible representation of the euclidean motion group. International Journal of Computer Vision **72**(1), 79–102 (2007). DOI 10.1007/s11263-006-8894-5
24. Duits, R., Franken, E.: Left-invariant parabolic evolutions on $SE(2)$ and contour enhancement via invertible orientation scores. Part I: linear left-invariant diffusion equations on $SE(2)$. Quarterly of Applied Mathematics **68**(2), 255–292 (2010)
25. Faugeras, O., Touboul, J., Cessac, B.: A constructive mean-field analysis of multi-population neural networks with random synaptic weights and stochastic inputs. Frontiers in computational neuroscience **3**, 1 (2009). DOI 10.3389/neuro.10.001.2009
26. Franceschiello, B., Mashtakov, A., Citti, G., Sarti, A.: Modelling of the poggendorff illusion via sub-riemannian geodesics in the roto-translation group. In: International Conference on Image Analysis and Processing, pp. 37–47. Springer (2017)
27. Franceschiello, B., Mashtakov, A., Citti, G., Sarti, A.: Geometrical optical illusion via sub-riemannian geodesics in the roto-translation group. Differential Geometry and its Applications **65**, 55–77 (2019)
28. Franceschiello, B., Sarti, A., Citti, G.: A neuromathematical model for geometrical optical illusions. Journal of Mathematical Imaging and Vision **60**(1), 94–108 (2018)
29. Howe, C.Q., Yang, Z., Purves, D.: The poggendorff illusion explained by natural scene geometry. Proceedings of the National Academy of Sciences **102**(21), 7707–7712 (2005)
30. Hubel, D.H., Wiesel, T.N.: Receptive fields and functional architecture of monkey striate cortex. The Journal of physiology **195**(1), 215–243 (1968)
31. Kim, J., Batard, T., Bertalmío, M.: Retinal processing optimizes contrast coding. Journal of Vision **16**(12), 1151–1151 (2016)
32. Kitaoka, A.: Adelsons checker-shadow illusion-like gradation lightness illusion. http://www.psy.ritsumei.ac.jp/~akitaoka/gilchrist2006mytalke.html (2006). Accessed: 2018-11-03
33. Martinez-Garcia, M., Cyriac, P., Batard, T., Bertalmío, M., Malo, J.: Derivatives and inverse of cascaded linear+nonlinear neural models. PLOS ONE **13**(10), 1–49 (2018)
34. McCourt, M.E.: A spatial frequency dependent grating-induction effect. Vision Research **22**(1), 119 – 134 (1982)
35. Olshausen, B.A., Field, D.J.: Vision and the coding of natural images: The human brain may hold the secrets to the best image-compression algorithms. American Scientist **88**(3), 238–245 (2000)
36. Otazu, X., Vanrell, M., Parraga, C.A.: Multiresolution wavelet framework models brightness induction effects. Vision Research **48**(5), 733 – 751 (2008)
37. Petitot, J.: Elements of Neurogeometry: Functional Architectures of Vision. Lecture Notes in Morphogenesis. Springer International Publishing (2017)
38. Prandi, D., Gauthier, J.P.: A semidiscrete version of the Petitot model as a plausible model for anthropomorphic image reconstruction and pattern recognition. SpringerBriefs in Mathematics. Springer International Publishing, Cham (2017)
39. Rucci, M., Victor, J.D.: The unsteady eye: an information-processing stage, not a bug. Trends in neurosciences **38**(4), 195–206 (2015)
40. Sarti, A., Citti, G.: The constitution of visual perceptual units in the functional architecture of V1. J. Comput. Neurosci. **38**(2), 285–300 (2015). DOI 10.1007/s10827-014-0540-6
41. Self, M.W., Lorteije, J.A., Vangeneugden, J., van Beest, E.H., Grigore, M.E., Levelt, C.N., Heimel, J.A., Roelfsema, P.R.: Orientation-tuned surround suppression in mouse visual cortex. Journal of Neuroscience **34**(28), 9290–9304 (2014)
42. Ts'o, D.Y., Gilbert, C.D., Wiesel, T.N.: Relationships between horizontal interactions and functional architecture in cat striate cortex as revealed by cross-correlation analysis. Journal of neuroscience **6**(4), 1160–1170 (1986)
43. Veltz, R., Faugeras, O.: Local/global analysis of the stationary solutions of some neural field equations. SIAM Journal on Applied Dynamical Systems **9** (2009). DOI 10.1137/090773611
44. Webster, M.A.: Visual adaptation. Annual Review of Vision Science **1**(1), 547–567 (2015). DOI 10.1146/annurev-vision-082114-035509. PMID: 26858985
45. Weintraub, D.J., Krantz, D.H.: The Poggendorff illusion: amputations, rotations, and other perturbations. Attention Perception & Psychophysics **10(4)**, 257–264 (1971)
46. Westheimer, G.: Illusions in the spatial sense of the eye: geometrical-optical illusions and the neural representation of space. Vision Research **48(20)**, 212–2142 (2008)

47. White, M.: A new effect of pattern on perceived lightness. Perception **8**(4), 413–416 (1979)
48. Wilson, H.R., Cowan, J.D.: Excitatory and inhibitory interactions in localized populations of model neurons. BioPhysics Journal **12**(1) (1972)
49. Yeonan-Kim, J., Bertalmío, M.: Retinal lateral inhibition provides the biological basis of long-range spatial induction. PLOS ONE **11**(12), 1–23 (2016)
50. Zhang, J., Duits, R., Sanguinetti, G., ter Haar Romeny, B.M.: Numerical approaches for linear left-invariant diffusions on se (2), their comparison to exact solutions, and their applications in retinal imaging. Numerical Mathematics: Theory, Methods and Applications **9**(1), 1–50 (2016)